JAAS

ROYAL SOCIETY OF CHEMISTRY

TECHNICAL NOTE

View Article Online
View Journal | View Issue

Cite this: *J. Anal. At. Spectrom.*, 2025, **40**, 326

Three new natural secondary reference materials for *in situ* andradite U–Pb geochronology†

Yueheng Yang, *[a] Shitou Wu, [a] Hao Wang,[a] Sandra L. Kamo,[b] Qian Ma,[c] Ting Liang,[d] Lei Xu,[a] Liewen Xie, [a] Chao Huang, [a] Bo Wan,[a] Jinhui Yang[a] and Fuyuan Wu[a]

Received 11th August 2024
Accepted 3rd December 2024

DOI: 10.1039/d4ja00290c

rsc.li/jaas

Andradite-rich garnet is a common mineral found in various rock types, such as alkaline igneous rocks and skarns, and often exhibits high U/Pb ratios, making it suitable for *in situ* U–Pb dating. However, the limited availability of well-characterised andradite reference materials has impeded their broader application in microanalysis. In this study, three natural andradite samples (MKWB, DGS, and Stanley) have been characterised and assessed as potential secondary reference materials for *in situ* U–Pb geochronology. U–Pb isotopic analyses were conducted across four different laboratories using isotope dilution – TIMS, SIMS, and laser ablation (SF, Q)-ICP-MS, to examine the homogeneity of the euhedral andradite crystals. We report ID-TIMS $^{206}Pb/^{238}U$ ages of 264.9 ± 5.8 Ma (2 s, n = 6, MSWD = 3.4), 139.42 ± 0.36 Ma (2 s, n = 5, MSWD = 1.9), and 23.28 ± 0.38 Ma (2 s, n = 3, MSWD = 1.9) for MKWB, DGS, and Stanley, respectively. These three newly characterised natural secondary reference materials should significantly contribute to the advancement of *in situ* U–Pb andradite-rich garnet geochronology.

1. Introduction

Grandite garnets form a solid-solution series between andradite and grossular and are widely found in various alkaline magmatic rocks,[1,2] carbonatites, and skarn deposits, often associated with economically significant Fe, Cu, W, Sn, and Mo mineralisation.[3,4] Garnet has the unique ability to record the conditions and timing of its growth through its major, trace element, and isotopic characteristics. Consequently, grandite garnet geochronology holds the potential to provide direct constraints on the timing of magma emplacement and hydrothermal processes.[4–8]

Although the potential for U–Pb dating of grossular–andradite garnet has long been recognised, the low-U content of grandite garnet, often with abundant inclusions, poses challenges, and only a few successful applications have been documented.[9,10] The Sm–Nd and Lu–Hf isotopic systems are most commonly used for garnet age determination through isotope dilution (ID) thermal ionisation mass spectrometry (TIMS) or multiple collector inductively coupled plasma mass spectrometry (MC-ICP-MS).[11] Recently, *in situ* Lu–Hf geochronology of garnet using Tandem with ICP coupled with laser ablation (LA-ICP-MS/MS) has shown promising results.[12,13] However, routine *in situ* Lu–Hf dating of garnet remains challenging due to the low Lu content, particularly in younger grains (<500 Ma). In contrast, *in situ* U–Pb methods such as LA-ICP-MS or secondary ion mass spectrometry (SIMS) do not require a co-genetic phase or whole rock measurement to calculate an age.

Recently, grossular–andradite garnet, similar to other low U-bearing minerals such as wolframite, cassiterite, and calcite,[14–17] has seen increased use in *in situ* U–Pb geochronology.[3–6] For instance, Seman *et al.*[6] were the first to present *in situ* U–Pb geochronology of grossular–andradite garnet using LA-ICP-MS. Deng *et al.*[5] confirmed the feasibility of garnet U–Pb geochronology using zircon (91 500) as the external calibration standard with optimised instrumental parameters. Similarly, Ti-bearing andradite, schorlomite, characterised by relatively higher U content and low common Pb, has shown even greater potential for U–Pb geochronology.[3,7,8] Since then, applications of andradite U–Pb dating have been published, with important implications for understanding the timing and rate of processes such as magma emplacement and hydrothermal activity.[8,18–20]

While many LA-ICP-MS studies have demonstrated that matrix effects can be minimised through optimised laser parameters and data reduction strategies,[4,5,21] the use of U–Pb reference materials with the same mineral compositions is preferable and essential for both ion and laser probe microanalysis. Currently, only a few matrix-matched U–Pb garnet

[a]*State Key Laboratory of Lithospheric and Environmental Coevolution, Institute of Geology and Geophysics, Chinese Academy of Sciences, P. B. 9825, Beijing, 100029, China. E-mail: yangyueheng@mail.iggcas.ac.cn*

[b]*Jack Satterly Geochronology Laboratory, Department of Earth Sciences, University of Toronto, 22 Ursula Franklin Street, Toronto, Ontario, M5S 3B1, Canada*

[c]*Institute of Geology, Chinese Academy of Geological Sciences, Beijing, 100037, China*

[d]*School of Earth and Space Science, University of Science and Technology of China, Hefei, 230026, China*

† Electronic supplementary information (ESI) available. See DOI: https://doi.org/10.1039/d4ja00290c

reference materials are available. For example, Willsboro andradite (~1 ppm U) and Mali grandite (2–7 ppm U) were first developed as primary and secondary reference materials due to their negligible initial common Pb.[6] Meanwhile, QC-4 andradite and WS20 schorlomite have been used as in-house U–Pb reference materials, although TIMS ages are not yet available for them.[3,5] Recently, Salnikova *et al.*[7] presented several calcic garnets from carbonatitic and alkaline rocks as geochronological and petrogenetic tools applicable to a wide variety of rock types. More recently, PL57 schorlomite, with ~40 ppm U content, has been proposed as a potential U–Pb primary reference material,[8] while ICU-1, Jumbo, and Tiptop andradites have been presented as U–Pb reference materials.[22,23] However, other andradite reference materials for O isotope analysis have not reported their U–Pb ages.[24]

In this study, conducted in three separate LA-ICP-MS laboratories, both TIMS and SIMS laboratories, we present three new secondary reference materials—MKWB, DGS, and Stanley—which can be used for *in situ* U–Pb geochronology. The primary objectives of this study are: (i) to examine the elemental and isotopic homogeneity of the three samples; (ii) to evaluate the feasibility of these samples as secondary U–Pb reference materials.

2. Samples and methods

All andradite samples investigated in this study were sourced from a commercial dealer or obtained through colleagues. The U–Pb age measurements using TIMS, SIMS or LA-ICP-MS were carried out in four laboratories: the Jack Satterly Geochronology Laboratory, Department of Earth Sciences, University of Toronto (JGL-DES-UT) in Toronto; the Institute of Geology and Geophysics, Chinese Academy of Sciences (IGG-CAS) in Beijing; the Institute of Geology, Chinese Academy of Geological Sciences (IG-CAGS) in Beijing; and the School of Earth and Space Science, University of Science and Technology of China (SESS-USTC) in Hefei.

2.1 Sample descriptions

Willsboro andradite originates from the Willsboro wollastonite deposit in the Adirondack Highlands Province, USA. Its composition closely aligns with that of end-member andradite, with an Adr_{82}–Grs_{18} ratio, and it does not exhibit observable oscillatory growth zonation. Concordia U–Pb ages of 1022 ± 16 Ma (ref. 6) and 1024.7 ± 9.6 Ma (ref. 23) have been obtained using ID-TIMS in different laboratories. This sample has been widely used as a primary reference material for U–Pb dating in many LA-ICP-MS analyses. The fragments used in this study are from the same location as those analysed by Seman *et al.*[6] The garnets comprise much of the matrix, appearing as somewhat granular, orange-brown aggregates densely intergrown with minor green diopside and white wollastonite. A rich, classic sample has a size of about 8 × 7 × 4 cm. The relatively high uncertainty in the age might be attributed to the low uranium content (~1 ppm).

Mali grandite is sourced from alluvial deposits in southern Mali. The grains are dark red, euhedral garnet crystals with an average composition of Adr_{55}-Grs_{42}, containing a higher uranium content of 2–7 ppm. Oscillatory zoning is not evident, and no inclusions were detected in optical and backscattered electron (BSE) images. U–Pb dating results obtained by ID-TIMS and LA-ICP-MS yielded ages of 202.2 ± 1.2 Ma and 202.0 ± 2.0 Ma, respectively. The crystals show excellent dodecahedral faces and are quite large, with some showing modest etching and recrystallization on some faces. Fine single crystals average about 4 cm in height. This specimen is commonly used as a quality monitor for routine LA-ICP-MS analysis.[6]

MKWB andradite comes from the Mengku large-scale iron deposit in Maizi Basin, southern Altay, Xinjiang, western China. Its composition is close to that of end-member andradite, with an Adr_{80}–Grs_{15} ratio, and it does not display observable oscillatory growth zonation (Fig. 1a). The grains are unusually yellowish coloured andradite garnets, often exceeding 2 cm, intergrown and showing fine decahedral faces (Fig. 1b). Previous U–Pb dating of hydrothermal zircon from the skarn (250 ± 2 Ma)[25,26] and Re–Os dating of molybdenite-bearing quartz veins (261 ± 7 Ma) have been reported.[27]

DGS andradite is from the Dongguashan skarn copper deposit in the Tongling area, Anhui, eastern China (Fig. 1c and d). It shows no apparent oscillatory zonation, and no inclusions were observed in optical and BSE images. Previous U–Pb dating of magmatic zircon (138.0 ± 1.7 Ma) has been reported.[28,29]

Stanley andradite is from Stanley Butte, located on the San Carlos Indian Reservation in Graham County, Arizona, USA. It occurs as a gangue mineral in a skarn deposit, forming euhedral crystals on the walls of a hydrothermal vein (Fig. 1c). The grains are unusually yellowish coloured andradite garnets, often exceeding 1 cm or more, with overall sizes ranging from about 5 cm, mostly closely intergrown and displaying fine decahedral faces in these colourful specimens.[30] There are no available reference age data for this sample (Fig. 1f).

2.2 Major and trace element analysis

Major element analysis and BSE imaging were conducted using a CAMECA SX Five Electron Microprobe housed at IGG-CAS. The operating conditions included a beam current of 3×10^{-8} A with an acceleration voltage of 15 kV and a beam diameter of 5 μm. The peak counting time was 20 seconds for all elements, with a background counting time of 10 seconds on both the high- and low-energy background positions. Natural and synthetic minerals were used for standardization, and the minerals were routinely analysed for Mg, Ca, Mn, Fe, Al, Cr, Si, and Ti.

Trace element measurements were carried out using a Thermo Scientific Element XR Sector Field (SF) ICP-MS, coupled with a 193 nm ArF excimer laser at IGG-CAS. The BCR-2G/ARM-2 reference material was simultaneously analysed with every ten samples. External calibration was performed relative to ARM-2 glass using the values recommended by Wu *et al.*[31] with internal standardization based on Si content. The accuracy and precision of the analyses were evaluated using BCR-2G, with results consistently better than 10% combined. Trace element data reduction was carried out using Iolite

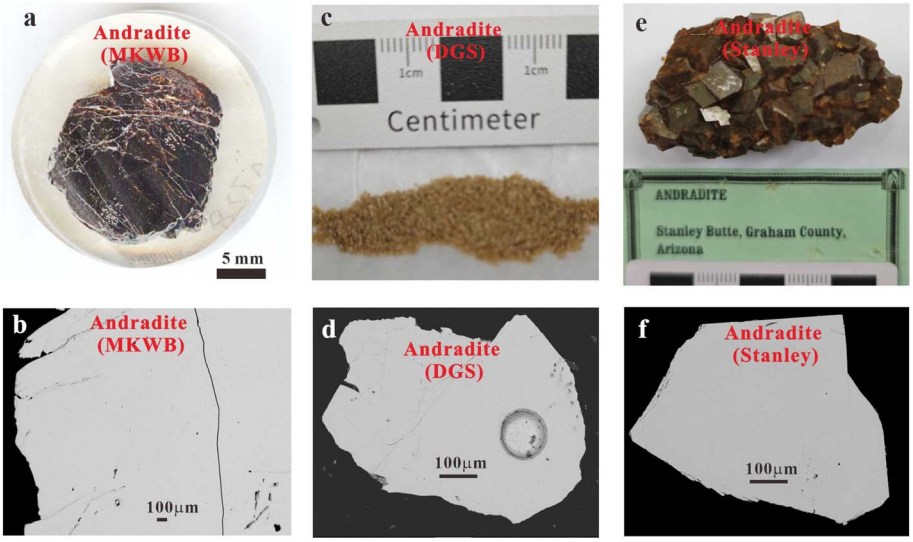

Fig. 1 Representative photographs of MKWB (a), DGS (c) and Stanley (e) andradite samples. False-colour back-scattered electron (BSE) images of the investigated andradite samples MKWB (b), DGS (d), and Stanley (f), show no compositional zoning.

software.[32] The rare earth element (REE) patterns of andradite were normalized to chondritic values.[33]

2.3 ID-TIMS U–Pb measurement

Separate andradite mineral samples were dated using ID-TIMS U–Pb geochronology at JGL-DES-UT. Each grain was washed in 8 N nitric acid (HNO_3) at room temperature, then loaded into Teflon dissolution capsules with approximately 120 μL of 50% hydrofluoric acid and around 20 μL of HNO_3, along with a mixed ^{205}Pb–^{235}U isotopic tracer solution, and heated at 195 °C for about four days. The samples were dried to a precipitate and re-dissolved in approximately 0.15 mL of 3.1 N HCl before being loaded into anion exchange columns.[34] An HBr chemical separation procedure was used to isolate Pb and U, which were then evaporated to a small droplet in H_3PO_4 and loaded onto outgassed rhenium filaments with silica gel.[35]

U and Pb were analysed using a VG354 mass spectrometer, utilising either a Daly detector in pulse counting dynamic mode or multiple Faraday cups in static measurement mode, with ^{204}Pb measured using the axial Daly detector. Data acquisition was managed using either VG Sector software or an in-house Visual Basic program. Corrections to the $^{206}Pb/^{238}U$ and $^{207}Pb/^{206}Pb$ ages were made for the initial ^{230}Th disequilibrium, assuming a Th/U ratio of 4.2 in the magma. Initial common Pb was corrected using the Pb evolution model of Stacey and Kramers,[36] assuming a Pb procedural blank of 1 pg Pb and 0.1 pg U. The mass discrimination correction for the Daly detector was constant at 0.05% per atomic mass unit. Amplifier gains and Daly characteristics were monitored using the SRM 982 Pb reference material. Decay constants used were those reported by Jaffey *et al.*[37]: the decay constants of ^{238}U and ^{235}U were 1.55125×10^{-10} y and 9.8485×10^{-10} y, respectively. A $^{238}U/^{235}U$ ratio of 137.88 (ref. 38) was used for the $^{207}Pb/^{206}Pb$ model age and $^{207}Pb/^{235}U$ age calculations. U–Pb data reduction and age calculations were performed using in-house Visual Basic programs developed by D. W. Davis. All age errors quoted in the text and table, as well as error ellipses in the concordia diagram, are given at the 95% confidence interval.

2.4 *In situ* U–Pb measurement

2.4.1 LA-SF-ICP-MS at IGG-CAS. *In situ* U–Pb isotope analyses were performed using an Element XR SF-ICP-MS coupled with a GeoLasPro 193 nm ArF excimer laser at IGG-CAS.[39,40] The system was optimised to achieve low oxide production rates ($ThO^+/Th^+ < 0.5\%$), low double-charged ions ($Ca^{2+}/Ca^+ < 1.0\%$), and robust plasma conditions (U^+/Th^+ ranging from 0.95 to 1.05) using ARM-2 while maximising signal-to-noise ratios. Isotopes including ^{202}Hg, ^{204}(Pb + Hg), ^{206}Pb, ^{207}Pb, ^{208}Pb, ^{232}Th, and ^{238}U were analysed by cycling the electrostatic analyser with a static magnet mass. Laser sampling was conducted using a fluence of approximately 3 J cm^{-2}, a spot size of 44 μm, and a repetition rate of 5 Hz. Prior to each analysis, a pre-ablation run using a 90 μm spot size for 2 seconds was performed to remove surface contamination from the andradite. Each spot measurement consisted of approximately 15 seconds of background acquisition followed by 45 seconds of data acquisition, consistent with procedures for low-U minerals (*e.g.*, wolframite,[14,15] cassiterite,[16] and calcite[17,40]). Usually, the ^{238}U sensitivity of ARM glass is 40–60 thousand counts per second with daily optimized parameters. The raw data were exported and processed offline using Iolite software to calculate Pb, Th, U content, and U–Pb age.[17] Willsboro was used as the primary U–Pb reference material, showing systematic downhole fractionation correction, while Mali was used as a secondary reference material.

2.4.2 LA–Q–ICP–MS at IG–CAGS. *In situ* U–Pb analyses were carried out using an Agilent 7900 quadrupole ICP–MS coupled with an ESI NWR 193 nm ArF excimer laser at IG–CAGS. The laser fluence, spot size, and repetition rate were set to 3 J cm^{-2}, 110 μm, and 10 Hz, respectively. The He carrier gas flows were

optimised by ablating NIST 612 glass to achieve maximum signal intensity for $^{238}U^+$ while maintaining a ThO^+/Th^+ ratio of <0.7% and a U/Th ratio close to 1. Usually, using 50 μm and 10 Hz, the ^{238}U sensitivity is ~40 thousand counts per second for NIST 612 glass under daily optimized parameters. Each analysis included approximately 20–30 seconds of background acquisition followed by 50 seconds of data acquisition, during which ^{202}Hg, ^{204}(Pb + Hg), ^{206}Pb, ^{207}Pb, ^{208}Pb, ^{232}Th, and ^{238}U were measured with dwell times of 10, 10, 20, 20, 10, 20, and 20 ms, respectively. Data reduction was performed offline using Iolite 3 software. Willsboro andradite was employed as the primary external standard for correcting the background, elemental/isotopic fractionation, and instrumental drift, while Mali grandite was analysed alternately as an unknown sample during analytical sessions.

2.4.3 LA-Q-ICP-MS at SESS-USTC. U–Pb dating of andradite was conducted using an Agilent 7900 quadrupole ICP-MS coupled with a GeoLas HD 193 nm ArF excimer laser at SESS-USTC. The laser had a diameter of 120 μm, an energy density of approximately 4 J cm^{-2}, and a frequency of 6 Hz. The He carrier gas flows were optimised by ablating NIST 612 glass to achieve maximum signal intensity for $^{238}U^+$ while maintaining a ThO^+/Th^+ ratio of <0.2% and a U/Th ratio close to 1. Usually, the ^{238}U sensitivity of NIST 612 is ~16 thousand counts per second for using 44 μm and 10 Hz with daily optimized parameters. Each single-spot analysis consisted of 20 seconds of background signal acquisition followed by 50 seconds of laser ablation, during which ^{202}Hg, ^{204}(Pb + Hg), ^{206}Pb, ^{207}Pb, ^{208}Pb, ^{232}Th, and ^{238}U were measured with dwell times of 6, 20, 20, 30, 15, 10, and 15 ms, respectively. Willsboro andradite was used as the primary reference material, while Mali andradite served as the monitor quality material. Data reduction was performed offline using Iolite 4 software to determine trace element concentrations and U–Pb ages.[41]

2.4.4 SIMS at IGG-CAS. U–Pb analyses were performed using a CAMECA IMS1280HR. An O_2^- primary ion beam was accelerated at ~13 kV potential. The beam spot was around 25 × 35 μm^2 in size with an elliptical shape. It has been a common procedure to introduce high purity oxygen gas onto the sample surface (oxygen flooding) to enhance the yield of Pb^+ during SIMS U–Pb analysis on other accessory minerals such as baddeleyite and zircon. Considering the low U content of most andradite samples (mostly <10 ppm), we chose UO^+ and UO^{2+}, which show much higher yields than U^+ as the analytical ions to improve the analytical precision. In order to improve the precision of Pb isotope measurement, a dynamic multi-collector mode was adopted. Compared with the conventional mono-collector U–Pb dating method, the multi-collector mode can collect the signals of ^{204}Pb, ^{206}Pb, ^{207}Pb and ^{208}Pb simultaneously, which greatly improves the integration time of each signal and reduces the impact of primary ion beam fluctuations.[19]

The yield efficiency correction between different EMs is the prerequisite for Pb isotope measurement in dynamic multi-collector mode. This study took the C cup that collected ^{206}Pb as the benchmark and used the NIST 610 with high Pb content and well-known Pb isotope composition as the standard. Furthermore, the efficiency of other cups relative to the C cup was calibrated through multi-spot analyses. In order to avoid the possible Pb isotope fractionation caused by matrix variation, $^{207}Pb/^{206}Pb$ ratios of the andradite Willsboro reference material were used to further calibrate the relative efficiency between the C cup and H1 cup that collected ^{206}Pb and ^{207}Pb, respectively. The signal collection procedure includes 5 peak jumps: first, the matrix peak Fe_3O^+ (C cup); second, ^{204}Pb (L1), ^{206}Pb (C), ^{207}Pb (H1), and ^{208}Pb (H2); third, ThO^+ (L2) and UO^+ (C); then UO_2^+ (C); finally, CeO_2^+ (C). The counting time for each step is 1.04 s, 60 s, 8 s, 8 s, and 0.96 s and the waiting time is 3.6 s, 1.84 s, 2.4 s 1.52 s, and 4 s, respectively. Before data acquisition, each spot was pre-sputtered over a square area (25 × 25 μm) for 120 s to reduce the sample surface contamination. Each measurement consisted of 7 cycles with a total analytical time of ~16 min.[19]

3. Results and discussion

In this study, the ID-TIMS U–Pb analytical results for andradite samples are summarised in Table 1. The U–Pb ages of the andradite samples are depicted in Fig. 2–5 and reported in two different formats. Concordia diagrams for the ID-TIMS analysis are presented in Fig. 2. For the *in situ* U–Pb measurements (Table S1†), data with varying levels of common Pb are plotted in Tera–Wasserburg diagrams. Weighted mean $^{206}Pb/^{238}U$ ages were calculated using the ^{207}Pb correction, assuming a common Pb composition based on the two-stage crustal Pb model.[36] Lower-intercept U–Pb ages and weighted mean $^{206}Pb/^{238}U$ ages were determined using the Isoplot 3.23 software package.[42] Chondrite-normalised rare earth element (REE) data for Willsboro, Mali, MKWB, DGS, and Stanley andradite are plotted in Fig. 6. These data exhibit similar patterns and demonstrate a pronounced positive Eu anomaly, except for some Mali samples (see Table S2†).

3.1 ID-TIMS U–Pb measurement

Given the limited availability of andradite reference materials, we selected three samples—MKWB, DGS, and Stanley—for ID-TIMS U–Pb measurements based on our preliminary laser investigations. These samples were chosen due to their relatively lower $^{207}Pb/^{206}Pb$ ratios, moderate U contents, and/or homogeneous trace element compositions (Table 1).

Six aliquots of the MKWB andradite were analysed by ID-TIMS. The measured $^{206}Pb/^{204}Pb$ ratios for the MKWB sample range from 26 to 84. The total U contents vary between 1.4 μg g^{-1} and 1.7 μg g^{-1}, indicating U homogeneity. The U–Pb results are consistent within analytical uncertainty, yielding a corrected weighted average $^{206}Pb/^{238}U$ age of 264.9 ± 5.8 Ma (2 s, MSWD = 3.4; Fig. 2a). The corrected weighted average $^{207}Pb/^{235}U$ age of 269 ± 35 Ma (2 s, MSWD = 0.053) has a relatively large uncertainty, likely due to its lower U content, meanwhile, the main reason of the large uncertainties in some measurement for $^{207}Pb/^{206}Pb$ is too lower U content (~1.5 ppm U) and relatively younger age (Fig. 2a) and the accumulated radiogenic Pb is too lower. We prefer the weighted average $^{206}Pb/^{238}U$ age of 264.9 ± 5.8 Ma, which is in good agreement with previously reported Re–Os ages of 261 ± 7 Ma for molybdenite.[27]

Table 1 ID-TIMS U–Pb isotopic data for MKWB, DGS, Stanley andradite samples

					$^{206}Pb/^{204}Pb$	Atomic ratios							Apparent ages (Ma)						
Sample	Weight (mg)	U (μg g^{-1})	Th/U	Pb_C (pg)	Measured ratio	$^{207}Pb/^{235}U$	2σ	$^{206}Pb/^{238}U$	2σ	Rho	$^{207}Pb/^{206}Pb$	2σ	$^{207}Pb/^{235}U$	2σ	$^{206}Pb/^{238}U$	2σ	$^{207}Pb/^{206}Pb$	2σ	% Disc
MKWB																			
1	0.026	1.5	0.48	9.7	29	0.3218	0.1553	0.04391	0.00134	0.046	0.0531	0.0256	283	123	277.0	8.3	335	709	18
2	0.025	1.7	0.27	10.7	29	0.3183	0.3049	0.04284	0.00260	0.015	0.0549	0.0517	281	249	270.4	16.1	366	785	27
3	0.022	1.7	0.40	6.2	34	0.3056	0.1915	0.04230	0.00164	0.024	0.0524	0.0329	271	154	267.1	10.1	302	645	12
4	0.026	1.5	0.35	1.6	84	0.2987	0.0545	0.04186	0.00048	0.962	0.0517	0.0089	265	43	264.4	3.0	274	420	4
5	0.016	1.4	Na	3.5	35	0.3333	0.1515	0.04177	0.00131	0.031	0.0579	0.0263	292	119	263.8	8.1	525	1067	51
6	0.025	1.7	Na	13.1	26	0.2896	0.1824	0.03983	0.00156	0.710	0.0527	0.0321	258	147	251.8	9.7	317	929	21
DGS																			
1	0.026	11.7	Na	2.8	172	0.1488	0.0082	0.02196	0.00010	0.103	0.0492	0.0027	140.9	7.3	140.02	0.63	156	131	10
2	0.035	9.2	Na	1.9	259	0.1477	0.0042	0.02188	0.00008	0.205	0.0490	0.0014	139.9	3.7	139.53	0.50	146	66	4
3	0.039	12.2	0.01	1.1	617	0.1474	0.0017	0.02186	0.00004	0.516	0.0489	0.0005	139.6	1.5	139.38	0.28	144	25	3
4	0.051	23.1	0.49	1.9	875	0.1471	0.0029	0.02186	0.00006	0.520	0.0488	0.0009	139.4	2.5	139.37	0.38	139	43	0
5	0.040	10.8	0.01	0.9	701	0.1434	0.0030	0.02173	0.00014	0.475	0.0478	0.0009	136.0	2.6	138.59	0.90	91	44	−52
6	*0.041*	*14.3*	*0.00*	*1.1*	*762*	*0.1387*	*0.0035*	*0.02131*	*0.00035*	*0.700*	*0.0472*	*0.0009*	*131.9*	*3.1*	*135.96*	*2.23*	*59*	*43*	*−131*
Stanley																			
1	*0.034*	*5.3*	*0.45*	*2.0*	*40*	*0.0290*	*0.0084*	*0.003888*	*0.000084*	*0.154*	*0.0541*	*0.0155*	*29.0*	*8.3*	*25.02*	*0.54*	*376*	*698*	*94*
2	*0.034*	*5.3*	*0.15*	*1.6*	*46*	*0.0294*	*0.0052*	*0.003873*	*0.000062*	*0.189*	*0.0551*	*0.0097*	*29.4*	*5.1*	*24.92*	*0.40*	*416*	*409*	*94*
3	*0.061*	*5.2*	*0.02*	*0.9*	*107*	*0.0267*	*0.0020*	*0.003825*	*0.000019*	*0.910*	*0.0506*	*0.0036*	*26.7*	*2.0*	*24.61*	*0.12*	*222*	*166*	*89*
4	0.082	5.2	0.07	1.2	97	0.0206	0.0040	0.003613	0.000037	0.933	0.0414	0.0077	20.7	4.0	23.25	0.24	0	0	
5	0.070	5.6	0.01	1.1	104	0.0245	0.0020	0.003647	0.000037	0.563	0.0488	0.0038	24.6	2.0	23.47	0.24	137	183	83
6	0.043	5.9	0.04	1.2	67	0.0221	0.0031	0.003601	0.000032	0.776	0.0445	0.0060	22.2	3.1	23.17	0.21	0	10	

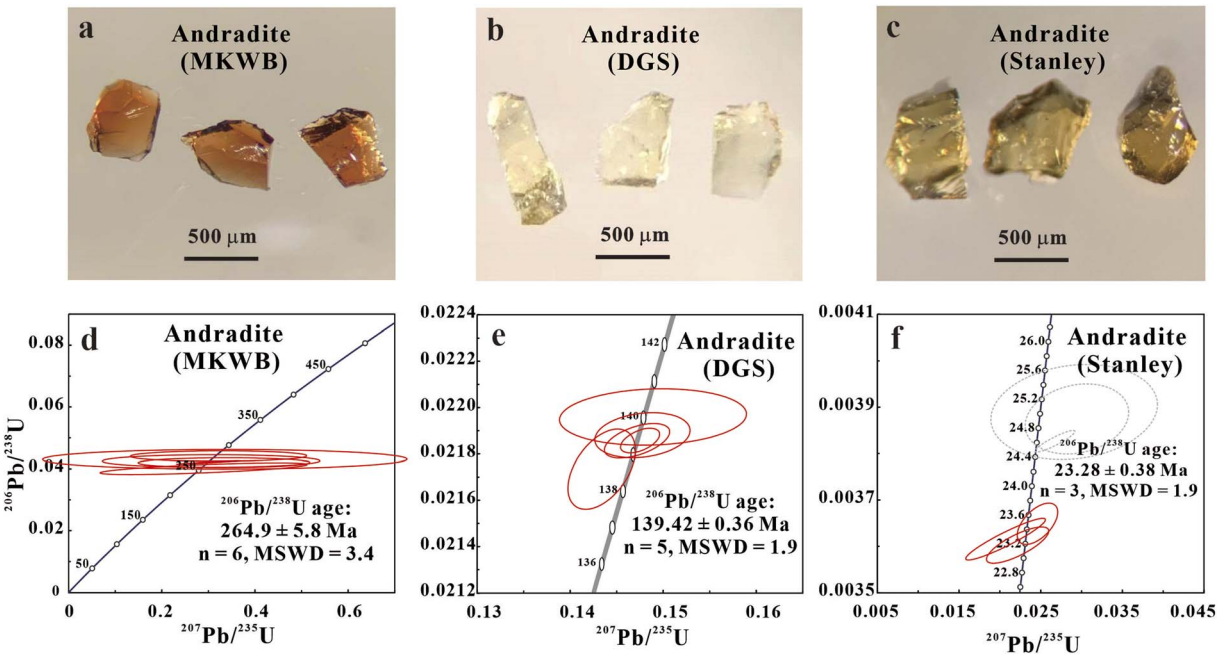

Fig. 2 The image of MKWB (a), DGS (b), Stanley (c) andradite chips for ID-TIMS in JGL-DES-UT. Concordia diagrams for ID-TIMS data of andradite samples (d) MKWB, (e) DGS, and (f) Stanley. Diagrams and ages are calculated using Isoplot (Ludwig, 2003). Error ellipses represent 2 s uncertainties.

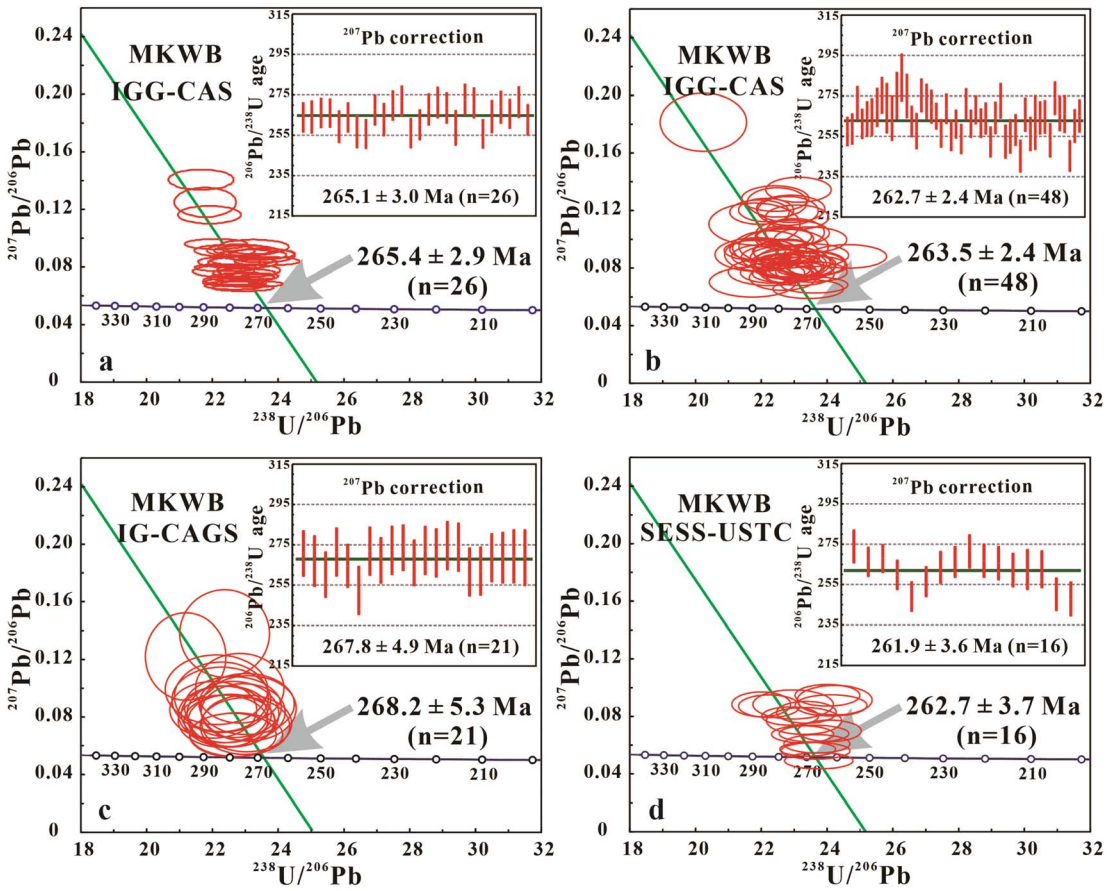

Fig. 3 LA-(Q, SF)-ICP-MS and SIMS U–Pb data of MKWB andradite samples from IGG-CAS (a and b), IG-CAGS (c), and SESS-USTC (d), respectively. The Tera–Wasserburg diagram and the ^{207}Pb corrected weighted average $^{206}Pb/^{238}U$ ages are shown. The green discordia lines in the Terra–Wasserburg diagrams are forced through a $^{207}Pb/^{206}Pb$ value of 0.85 ± 0.05 for the WKWB andradite sample. The $^{207}Pb/^{206}Pb$ values were estimated using the initial Pb isotope composition of sample MKWB by using the two-stage crustal Pb model of Stacey and Kramers (1975). Data were plotted and evaluated using Isoplot (Ludwig, 2003). Error bars in the insets are at the 1 s level.

The six fragments of DGS andradite exhibit heterogeneous U contents, ranging from 9.2 μg g^{-1} to 23.1 μg g^{-1}. The measured $^{206}Pb/^{204}Pb$ ratios vary from 172 to 875. The apparent $^{206}Pb/^{238}U$ ages for the five fragments range from 136.0 ± 2.6 to 140.9 ± 7.3 Ma, with a weighted average $^{206}Pb/^{238}U$ age of 139.42 ± 0.36 Ma (2 s, MSWD = 1.9; Fig. 2b). The corrected weighted average $^{207}Pb/^{235}U$ age of 139.0 ± 1.9 Ma (2 s, MSWD = 1.6) shows a relatively narrow uncertainty due to the higher U content. One outlier aliquot (6) may be influenced by common Pb-rich inclusions (such as sulphides) that were not fully removed during the leaching process. We prefer the weighted average $^{206}Pb/^{238}U$ age of 139.42 ± 0.36 Ma, which aligns well with previously reported U–Pb ages of 138.0 ± 1.7 Ma for zircon.[29]

The six fragments of Stanley andradite exhibit low U contents, ranging from 5.2 μg g^{-1} to 5.9 μg g^{-1}, suggesting U homogeneity. The measured $^{206}Pb/^{204}Pb$ ratios range narrowly from 40 to 104. The apparent $^{206}Pb/^{238}U$ ages of the three fragments range from 23.17 ± 0.21 to 23.47 ± 0.24 Ma, yielding a weighted average $^{206}Pb/^{238}U$ age of 23.28 ± 0.38 Ma (2 s, MSWD = 1.9; Fig. 3c). The corrected weighted average $^{207}Pb/^{235}U$ age of 23.4 ± 4.6 Ma (2 s, MSWD = 1.9) has a relatively large uncertainty, likely due to the lower U content. The three outlier aliquots (1, 2, 3) were excluded due to their lower measured $^{206}Pb/^{204}Pb$ ratios and apparent $^{206}Pb/^{238}U$ ages. The significant variation in measured $^{206}Pb/^{204}Pb$ values for the Stanley sample reflects the presence of Pb-rich inclusions that were not completely removed during the sample preparation using the dilute leaching process.

3.2 *In situ* U–Pb measurement

MKWB andradite exhibits relatively homogeneous low-U values of *ca.* 2 μg g^{-1} and contains very low common Pb with f_{206} varying from 2 to 10% (Table S1†). During analytical sessions at IGG-CAS, measurements on MKWB andradite using SIMS and LA-SF-ICP-MS yielded lower-intercept $^{206}Pb/^{238}U$ ages of 265.4 ± 2.9 Ma (2 s, $n = 26$) and 263.5 ± 2.4 Ma (2 s, $n = 48$), respectively with a weighted mean $^{206}Pb/^{238}U$ age of 265.1 ± 3.0 Ma (2 s, $n = 26$) and 262.7 ± 2.4 Ma (2 s, $n = 48$), respectively (Fig. 3a and b). At IG-CAGS, twenty-one spots were measured using LA-Q-ICP-MS, yielding a lower-intercept age of 268.2 ± 5.3 Ma (2 s) with a weighted mean $^{206}Pb/^{238}U$ age of 267.8 ± 4.9 Ma (2 s) (Fig. 3c). Sixteen spots were measured at SESS-USTC using LA-Q-ICP-MS, resulting in a lower-intercept age of 262.7 ± 3.7 Ma (2 s) and a weighted mean $^{206}Pb/^{238}U$ age of 261.9 ± 3.6 Ma (2 s) (Fig. 3d).

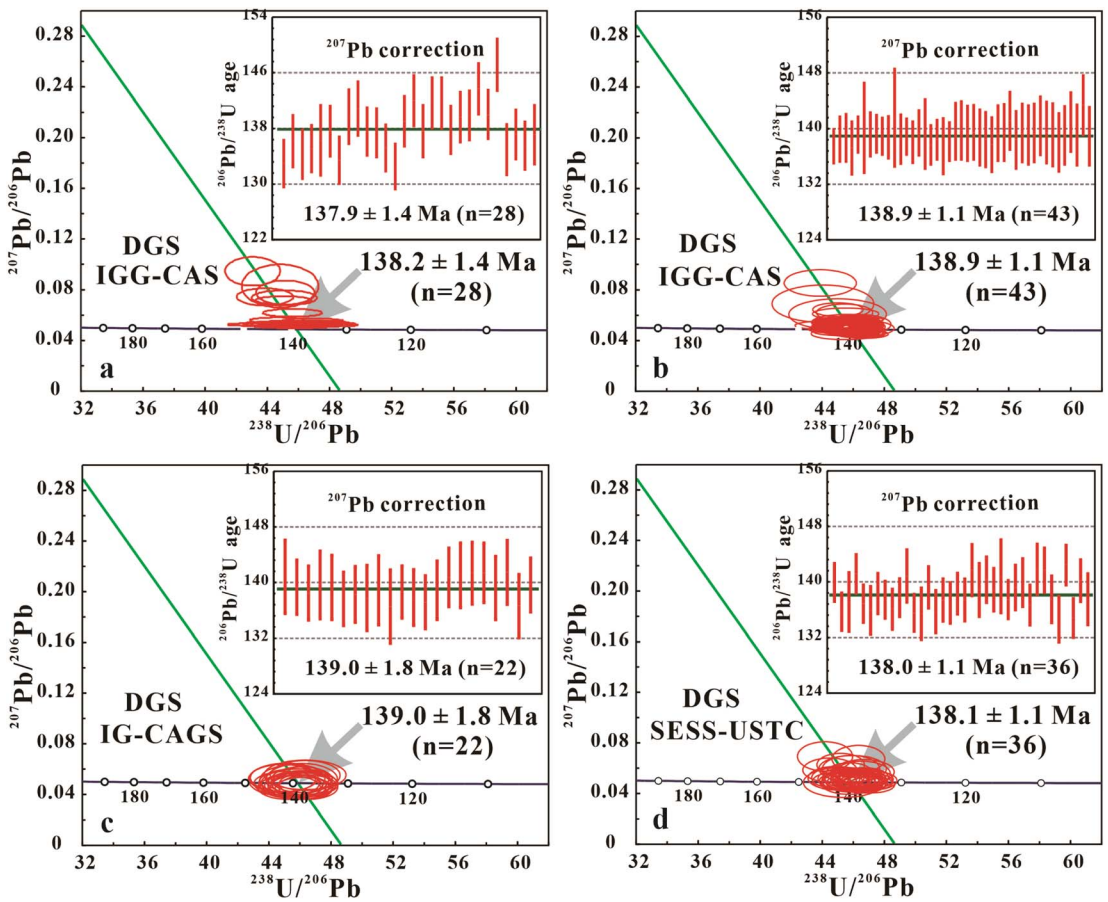

Fig. 4 LA-(Q, SF)-ICP-MS and SIMS U–Pb data of DGS andradite samples from IGG-CAS (a and b), IG-CAGS (c), and SESS-USTC (d), respectively. The Tera–Wasserburg diagram and the ^{207}Pb corrected weighted average $^{206}Pb/^{238}U$ ages are shown. The green discordia lines in the Terra–Wasserburg diagrams are forced through a $^{207}Pb/^{206}Pb$ value of 0.85 ± 0.05 for the DGS andradite sample. The $^{207}Pb/^{206}Pb$ values were estimated using the initial Pb isotope composition of sample MKWB by using the two-stage crustal Pb model of Stacey and Kramers (1975). Data were plotted and evaluated using Isoplot (Ludwig, 2003). Error bars in the insets are at the 1 s level.

These *in situ* values obtained from three laboratories are statistically consistent with the ID-TIMS mean $^{206}Pb/^{238}U$ age of 264.9 ± 5.8 Ma (2 s, $n = 6$).

DGS andradite shows relatively homogeneous high-U values between 5 and 10 μg g^{-1}, and contains negligible common Pb with f_{206} varying from 0 to 2% (Table S1†). The laser ablation U–Pb data from IGG-CAS during analytical sessions define intercept ages of 138.2 ± 1.4 Ma (2 s, $n = 28$) and 138.9 ± 1.1 Ma (2 s, $n = 43$), respectively, on the Tera–Wasserburg diagram. The corresponding ^{207}Pb corrected weighted mean $^{206}Pb/^{238}U$ ages are 137.9 ± 1.4 Ma (2 s, $n = 20$) and 138.9 ± 1.1 Ma (2 s, $n = 43$), respectively (Fig. 4a and b). At IG-CAGS, twenty-two spots were measured using LA-Q-ICP-MS, resulting in a lower-intercept age of 139.0 ± 1.8 Ma (2 s) with a weighted mean $^{206}Pb/^{238}U$ age of 139.0 ± 1.8 Ma (2 s) (Fig. 4c). At SESS-USTC, eighteen spots were measured using LA-Q-ICP-MS, yielding a lower-intercept age of 138.1 ± 1.1 Ma (2 s) with a weighted mean $^{206}Pb/^{238}U$ age of 138.0 ± 1.1 Ma (2 s) (Fig. 4d). The *in situ* U–Pb ages of DGS andradite obtained in these three laboratories are statistically consistent with the ID-TIMS age of 139.42 ± 0.36 Ma, also in good agreement with 138.0 ± 1.7 Ma for magmatic zircon.[29]

Stanley andradite shows more variable common Pb contributions than the other two samples in this study. The f_{206} values of Stanley range from 1 to 25% (Table S1†). The dataset of Stanley from analytical sessions at IGG-CAS yields intercept ages of 23.70 ± 0.31 Ma (2 s, $n = 29$) and 23.53 ± 0.43 Ma (2 s, $n = 46$) and ^{207}Pb corrected weighted mean $^{206}Pb/^{238}U$ ages of 23.30 ± 0.55 Ma (2 s, $n = 21$) and 23.33 ± 0.63 Ma (2 s, $n = 21$), respectively (Fig. 5a and b). At IG-CAGS, thirty spots were measured using LA-Q-ICP-MS, yielding a lower-intercept age of 22.91 ± 0.57 Ma (2 s) with a weighted mean $^{206}Pb/^{238}U$ age of 22.85 ± 0.54 Ma (2 s) (Fig. 5c). At SESS-USTC, twenty spots were measured using LA-Q-ICP-MS, resulting in a lower-intercept age of 23.86 ± 0.68 Ma (2 s, Fig. 5d) with a weighted mean $^{206}Pb/^{238}U$ age of 23.79 ± 0.67 Ma (2 s) (Fig. 5d). The *in situ* U–Pb ages of Stanley andradite obtained in these three laboratories are consistent with the ID-TIMS age of 23.28 ± 0.38 Ma.

3.3 Potential andradite reference materials for *in situ* U–Pb geochronology

Reference materials are the main benchmark for *in situ* U–Pb geochronology. Primary U–Pb reference materials with known ID-TIMS ages are usually characterised by relatively homogeneous, old ages (500–1000 Ma) or high U content, as well as negligible common Pb. Other known ID-TIMS U–Pb age

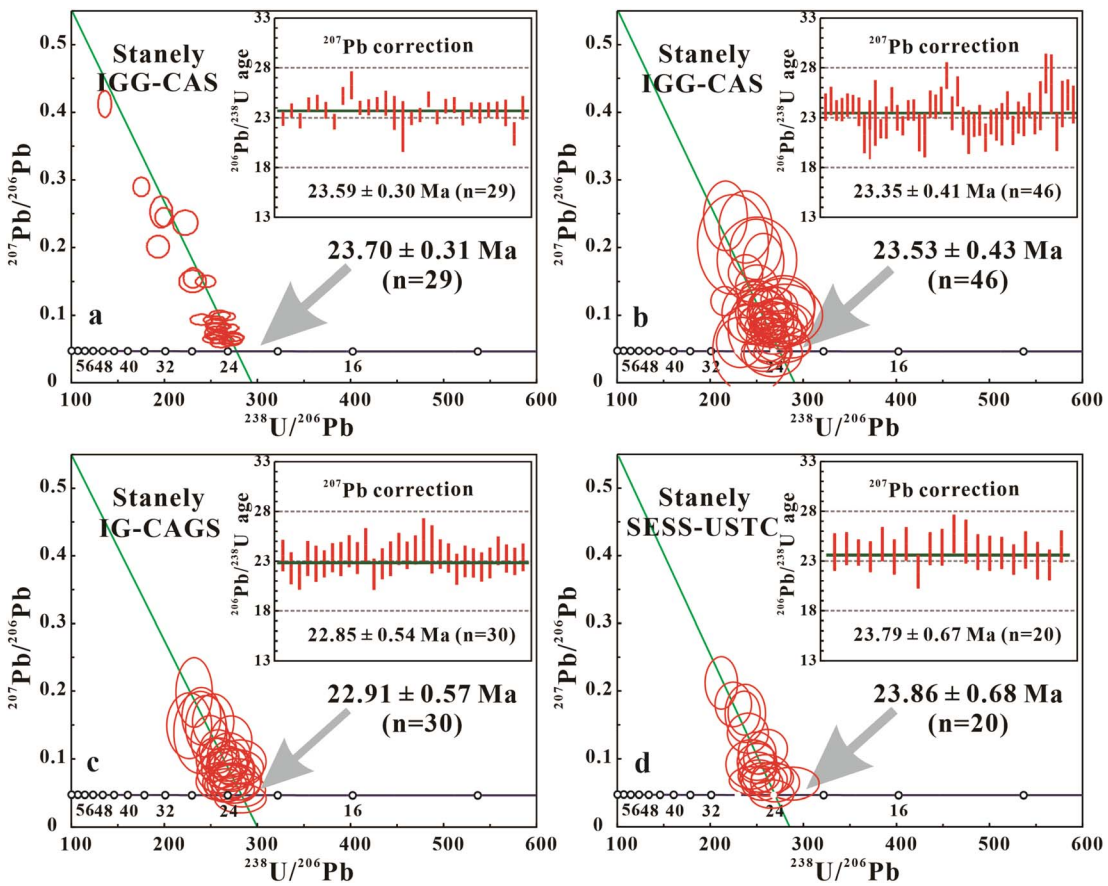

Fig. 5 LA-(Q, SF)-ICP-MS and SIMS U-Pb data of Stanley andradite samples from IGG-CAS (a and b), IG-CAGS (c), and SESS-USTC (d), respectively. The Tera–Wasserburg diagram and the ^{207}Pb corrected weighted average $^{206}Pb/^{238}U$ ages are shown. The green discordia lines in the Terra–Wasserburg diagrams are forced through a $^{207}Pb/^{206}Pb$ value of 0.84 ± 0.05 for the Stanley andradite sample. The $^{207}Pb/^{206}Pb$ values were estimated using the initial Pb isotope composition of sample Stanley by using the two-stage crustal Pb model of Stacey and Kramers (1975). Data were plotted and evaluated using Isoplot (Ludwig, 2003). Error bars in the insets are at the 1 s level.

Table 2 Compilation of available andradite reference materials for *in situ* U–Pb dating

Samples	U content (ppm)	$^{206}Pb/^{238}U$ age (±2 s) Ma (numbers)	Methods	References
Willsboro	1.10–1.85	1022 ± 16 (n = 9)	ID-TIMS	6
		1038 ± 19 (n = 11), 1041 ± 10 (n = 16)	SIMS	19
		1040 ± 16 (n = 40), 1019 ± 12 (n = 21)	LA-Q-ICP-MS	8
	1.45–2.27	1024.7 ± 9.6 (n = 6)	ID-TIMS	23
Mali	4.40–7.55	202.2 ± 1.2 (n = 4)	ID-TIMS	6
	~2	202.0 ± 2.0 (n = 25)	LA-SF-ICP-MS	6
		204.0 ± 3.0 (n = 10), 201.0 ± 2.0 (n = 17)	SIMS	19
		204.5 ± 1.9 (n = 15), 205.5 ± 2.1 (n = 14)	LA-Q-ICP-MS	8
		203.4 ± 0.8 (n = 75), 201.1 ± 1.4 (n = 19)	LA-SF-ICP-MS	22
QC-4	46.0–107	130 ± 1 (n = 32)	LA-Q-ICP-MS	5
		134.2 ± 3.2 (n = 29)	LA-Q-ICP-MS	8
		128.7 ± 0.7 (n = 20), 128.4 ± 0.9 (n = 47)	LA-SF-ICP-MS	22
		129.9 ± 1.4 (n = 20), 129.9 ± 0.4 (n = 41))	LA-Q-ICP-MS	22
WS20	10–40	1153 ± 10 (n = 10)	LA-Q-ICP-MS	3
		1156.2 ± 1.2 (n = 8)	SIMS	19
15 MC	10–19	96.4 ± 1.8 (n = 13)	LA-Q-ICP-MS	3
		97.0 ± 1.0 (n = 11), 94.2 ± 0.9 (n = 15)	SIMS	19
Afrikanda	14.1–16.5	377.5 ± 2.0 (n = 2)	ID-TIMS	7
Odikhincha	13.6–16.0	249.5 ± 1.0 (n = 2)	ID-TIMS	7
PL57	27–76	1156.2 ± 1.2 (n = 10)	ID-TIMS	8
ICU-1	26.67	20.57 ± 0.77 (n = 1)	ID-TIMS	22
		21.09 ± 0.20 (n = 42), 21.83 ± 0.24 (n = 37)	LA-SF-ICP-MS	22
		21.96 ± 0.30 (n = 46), 20.74 ± 0.11 (n = 81)	LA-Q-ICP-MS	22
ICU-2	28.15	20.88 ± 0.96 (n = 1)	ID-TIMS	22
		20.47 ± 0.26 (n = 74), 20.68 ± 2.68 (n = 42)	LA-SF-ICP-MS	22
		20.75 ± 3.42 (n = 14), 20.85 ± 3.54 (n = 86)	LA-Q-ICP-MS	22
Jumbo	24.4–113.6	110.34 ± 0.13 (n = 6)	ID-TIMS	23
Tiptop	1.29–3.52	209.57 ± 0.26 (n = 6)	ID-TIMS	23
MKWB	1.4–1.7	264.9 ± 5.8 (n = 6), 265.1 ± 3.0 (n = 26)	ID-TIMS, SIMS	This study
		262.7 ± 2.4 (n = 48)	LA-SF-ICP-MS	This study
		267.8 ± 4.9 (n = 21), 261.9 ± 3.6 (n = 16)	LA-Q-ICP-MS	This study
DGS	9.2–23.1	139.42 ± 0.36 (n = 5), 137.9 ± 1.4 (n = 28)	ID-TIMS, SIMS	This study
		138.9 ± 1.1 (n = 43)	LA-SF-ICP-MS	This study
		139.0 ± 1.8 (n = 22), 138.0 ± 1.1 (n = 36)	LA-Q-ICP-MS	This study
Stanley	5.2–5.9	23.28 ± 0.38 (n = 3), 23.59 ± 0.30 (n = 29)	ID-TIMS, SIMS	This study
		23.35 ± 0.41 (n = 46)	LA-SF-ICP-MS	This study
		22.85 ± 0.54 (n = 30), 23.79 ± 0.67 (n = 20)	LA-Q-ICP-MS	This study

samples are used as secondary reference materials for data quality monitoring during analytical sessions.[6,13–17] The available andradite reference materials for *in situ* U–Pb dating are summarised in Table 2 for comparison. The U–Pb ages of Willsboro and Mali andradites were initially determined and reported using ID-TIMS and LA-ICP-MS.[6] Willsboro andradite, characterised by negligible common Pb and homogeneous trace element composition (Fig. 6a), has been widely used as a primary reference material for *in situ* andradite U–Pb dating, despite its relatively low U content (1–2 ppm).[4] Similarly, Mali andradite, which is associated with the lowest common Pb and varying U content depending on its colour (*e.g.*, yellow and black), has been extensively used as a secondary reference material.[4,22,43] Although Mali andradites come from the same area, they show distinct compositional differences. We also dated Mali samples using the *in situ* U–Pb method over extended analytical sessions at IGG-CAS. Our laser ages are consistent with the previously reported age of ~202 Ma. Despite all Mali fragments being derived from a single crystal, the deviation is considerably larger than previously reported (less than 3%). This may reflect variations in common Pb contents within individual shards of the crystal, as well as among different shards (Fig. 6b). Therefore, special care, such as using back-scattered electron images, trace elements, and real-time mass spectrum signals, should be taken when using Mali as a reference material for *in situ* U–Pb dating.[22,43,44]

QC-4, provided by Deng *et al.*[5] is used as an in-house monitor sample due to the absence of a TIMS age.[22] Similarly, WS20 schorlomite, presented by Yang *et al.*,[3] is used as an in-house U–Pb reference material for both laser and ion probe analyses.[19] A recent ID-TIMS study on PL57 schorlomite from the same location yielded a concordant age of 1156.2 ± 1.2 Ma,[8] which is identical to the baddeleyite Pb–Pb age obtained using SIMS.[19] Consequently, this new TIMS age can be adopted as the recommended age for WS20 schorlomite.

Although U–Pb geochronological data for six Ca–Fe–Ti garnets from diverse alkaline and carbonatitic intrusive rocks (15 MC, Cinder Lake, Eden Lake, Belaya Zima, Afrikanda, and Odikhincha) have been obtained using ID-TIMS and their trace element compositions measured by LA-ICP-MS,[3,7] the feasibility and availability of these materials as U–Pb reference materials for microbeam analysis still require further demonstration and

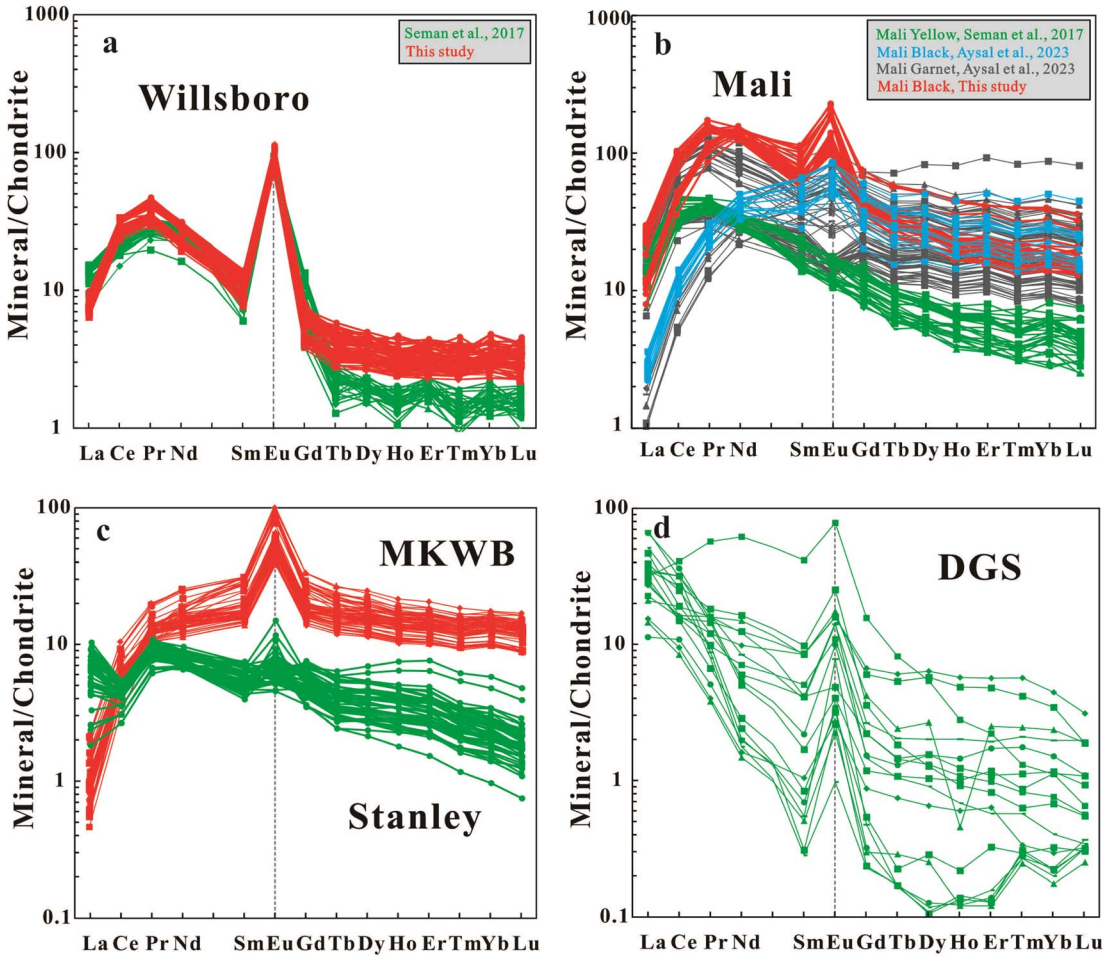

Fig. 6 The chondrite-normalized REE distribution patterns of individual andradite samples (Willsboro (a), Mali (b), MKWB (c), DGS (d) and Stanley (c)). Data from Seman *et al.*, 2017, Aysal *et al.*, 2023, and this study.

assessment. More recently, Aysal *et al.*[22] introduced IUC-1 as a new natural secondary reference material for garnet U–Pb dating by TIMS and LA-ICP-MS. Given its younger age, IUC-1 should be used as a quality monitor for younger samples. Similarly, the Jumbo and Tiptop reference materials, which have newly obtained ID-TIMS U–Pb ages, require further validation of their homogeneity for microanalysis.[23]

In this study, data from MKWB, DGS, and Stanley andradite have not been reported previously (Table 1). Based on available data, Ti-bearing andradite generally has a relatively higher U content compared to non-Ti-bearing andradite (*e.g.*, Willsboro and MKWB). MKWB, like Willsboro, is very homogeneous in terms of trace element composition (Fig. 6c), although it has a slightly lower U content (~2 ppm). Stanley, similar to IUC-1, is suitable as a secondary reference material during analytical sessions. DGS, with relatively higher U content, is suitable as a primary reference material despite its varied trace element composition (Fig. 6d). Both samples exhibit small variations in common Pb contents, resulting in f_{206} values of less than 5%. The U–Pb ages of MKWB obtained by LA-ICP-MS are consistent with ID-TIMS ages or published Re–Os ages,[27] making them suitable as secondary reference materials for andradite U–Pb dating. In contrast, sample Stanley contains high and variable common Pb contents and should therefore only be used for quality control of younger samples.

4. Conclusions

U–Pb ages of MKWB, DGS, and Stanley were determined, and their chemical compositions were characterized for evaluation as potential secondary reference materials in U–Pb geochronology. Testing was conducted in three laser laboratories and one TIMS/SIMS laboratory. We report the following ID-TIMS dating results for MKWB, DGS and Stanley andradite: $^{206}Pb/^{238}U$ ages of 264.9 ± 5.8 Ma (2 s, $n = 6$), 139.42 ± 0.36 Ma (2 s, $n = 5$) and 23.28 ± 0.38 Ma (2 s, $n = 3$) for MKWB, DGS and Stanley, respectively. MKWB like Mali, can be used as a secondary reference material for U–Pb age determinations and trace elements. DGS has a very homogeneous U–Pb age, while Stanley with an age of about 23 Ma is more suitable for use as a secondary reference material. Special care should be taken when using Mali as a secondary reference material because of its variable chemical composition. These three new natural

secondary reference materials should contribute significantly to the development of *in situ* U–Pb andradite geochronology.

Data availability

The data that support the findings of this study are available in the ESI† of this article. Crystals and fragments of MKWB, DGS and Stanley are available upon request for laboratories worldwide by contacting Prof. Y. H. Yang (E-mail: yangyueheng@mail.iggcas.ac.cn).

Author contributions

Conceptualization: Y. Y. Yang, S. T. Wu and H. Wang; formal analysis: S. L. Kamo, Q. Ma, and T. Liang; methodology: C. Huang, L. W. Xie, and L. Xu; writing – original draft: Y. H. Yang; review: B. Wan, J. H. Yang, and F. Y. Wu; funding acquisition: Y. H. Yang.

Conflicts of interest

The authors declare no conflict of interest.

Acknowledgements

This work was financially supported by the National Natural Science Foundation of China (Grants 42430105, 42473037 and 42403032). We are indebted to H. Zhao for mass spectrometric measurement at JDL-DES-UT, G. M. Li for providing the DGS sample, Y. Liu and X. X. Ling for technical support during SIMS measurement. We thank the editor and two anonymous referees for their thoughtful and constructive comments on the draft.

References

1 F. E. Huggins, D. Virgo and H. G. Huckenholz, *Am. Mineral.*, 1977, **62**, 646–665.
2 C. B. Smith, S. E. Haggerty, B. Chatterjee, A. Beard and R. Townend, *Lithos*, 2023, **182/183**, 102–113.
3 Y. H. Yang, F. Y. Wu, J. H. Yang, R. H. Mitchell, Z. F. Zhao, L. W. Xi, C. Huang, Q. Ma, M. Yang and H. Zhao, *J. Anal. At. Spectrom.*, 2018, **33**, 231–239.
4 Y. H. Chen, R. Z. Hu, T. G. Lan, H. Wang, Y. W. Tang, Y. H. Yang, Z. D. Tian and T. Ulrich, *Chem. Geol.*, 2021, **572**, 120198.
5 X. D. Deng, J. W. Li, T. Luo and H. Q. Wang, *Contrib. Mineral. Petrol.*, 2017, **172**, 71.
6 S. Seman, D. F. Stockli and N. M. McLean, *Chem. Geol.*, 2017, **460**, 106–116.
7 E. B. Salnikova, A. R. Chakhmouradian, M. W. Stifeeva, E. P. Reguir, A. B. Kotov, Y. D. Gritsenko and A. V. Nikiforov, *Lithos*, 2019, **338/339**, 141–154.
8 D. F. Li, Y. Fu, P. Hollings, R. H. Mitchell, S. Zurevinski, S. Kamo, R. Q. Zhang, Y. Zhang, Q. F. Liu, J. L. Liao, Y. J. Liang and X. M. Sun, *Contrib. Mineral. Petrol.*, 2022, **177**, 19.
9 C. T. Barrie, *Can. J. Earth Sci.*, 1990, **27**, 1451–1456.
10 C. P. DeWolf, C. J. Zeissler, A. N. Halliday, K. Mezger and E. J. Essene, *Geochim. Cosmochim. Acta*, 1996, **60**, 121–134.
11 E. F. Baxter and E. E. Scherer, *Elements*, 2013, **9**, 433–438.
12 A. Simpson, S. Gilbert, R. Tamblyn, M. Hand, C. Spandler, J. Gillespie, A. Nixon and S. Glorie, *Chem. Geol.*, 2021, **577**, 120299.
13 S. T. Wu, H. Wang, Y. H. Yang, J. L. Niu, Z. W. Lan, L. L. Zhang, C. Huang, L. W. Xie, L. Xu, J. H. Yang and F. Y. Wu, *J. Anal. At. Spectrom.*, 2023, **38**, 1285–1300.
14 M. Yang, Y. H. Yang, S. T. Wu, R. L. Romer, X. D. Che, Z. F. Zhao, W. S. Li, J. H. Yang, F. Y. Wu, L. W. Xie, C. Huang, D. Zhang and Y. Zhang, *J. Anal. At. Spectrom.*, 2020, **35**, 2191–2203.
15 Y. H. Yang, M. Yang, H. Wang, J. H. Yang and F. Y. Wu, *Sci. China Earth Sci.*, 2021, **64**, 187–190.
16 M. Yang, R. L. Romer, Y. H. Yang, S. T. Wu, H. Wang, J. R. Tu, H. Y. Zhou, L. W. Xie, C. Huang, L. Xu, J. H. Yang and F. Y. Wu, *Chem. Geol.*, 2022, **593**, 120754.
17 S. T. Wu, Y. H. Yang, N. M. W. Roberts, M. Yang, H. Wang, Z. W. Lan, T. Y. Li, L. Xu, C. Huang, L. W. Xie, J. H. Yang and F. Y. Wu, *Sci. China Earth Sci.*, 2022, **65**, 1146–1160.
18 M. Gevedon, S. Seman, J. D. Barnes, J. S. Lackey and D. F. Stockli, *Earth Planet. Sci. Lett.*, 2018, **498**, 237–246.
19 Y. S. Huang, W. H. Zhao, Y. Liu, Y. H. Yang, G. Q. Tang, Y. Li, X. H. Li, H. Zhao and Q. L. Li, *J. Anal. At. Spectrom.*, 2022, **37**, 1109–1118.
20 S. Yan, R. Zhou, H. C. Niu, Y. X. Feng, A. D. Nguyen, Z. H. Zhao, W. B. Yang, Q. D. Dong and J. X. Zhao, *Bull. Geol. Soc. Am.*, 2020, **132**, 1031–1045.
21 K. Jenkins, K. Goemann, I. Belousov, M. Morissette and L. Danyushevsky, *Geostand. Geoanal. Res.*, 2023, **47**, 267–295.
22 N. Aysal, M. Guillong, T. Bayanova, M. Fukuyama, N. Leonard, I. Yılmaz, E. Varol, F. S. Tuke, Y. K. Kadioglu, N. Hanilci, F. Uzun and E. Kaygısız, *Geostand. Geoanal. Res.*, 2023, **47**, 297–310.
23 C. J. Beno, J. S. Lackey, M. D. Schmitz, J. R. Bowman, M. A. Stearns, J. M. Bartley and D. P. Fernandez, *Geostand. Geoanal. Res.*, 2024, **48**, 909–925.
24 A. Vho, D. Rubatto, B. Putlitz and A. S. Bouvier, *Geostand. Geoanal. Res.*, 2020, **44**, 459–471.
25 B. Wan, W. J. Xiao, L. C. Zhang and C. M. Han, *Ore Geol. Rev.*, 2012, **44**, 136–147.
26 Z. J. Zhong, L. L. Dong, W. Liu, H. Zhao, X. S. Wang, K. D. Cai and B. Wan, *Sci. Rep.*, 2019, **9**, 10382.
27 F. Q. Yang, Z. X. Zhang, W. J. Qu, X. X. Geng, S. J. Lv, F. W. Chai, L. P. L. Jiang and F. Liu, *Acta Geol. Sin.*, 2011, **85**, 396–404.
28 Z. Zheng, Y. S. Du, Y. Cao, Z. W. Gao, S. Yang and D. Dong, *Acta Petrol. Mineral.*, 2012, **31**, 235–242.
29 W. M. Guo, J. J. Lu, S. Y. Jiang, R. Q. Zhang and S. J. Zhao, *Sci. China: Earth Sci.*, 2013, **56**, 993–1013.
30 H. F. Xu, S. Y. Jin, S. Y. Lee and P. E. Brown, *Am. Mineral.*, 2023, **108**, 572–583.
31 S. T. Wu, G. Woerner, K. P. Jochum, B. Stoll, K. Simon and A. Kronz, *Geostand. Geoanal. Res.*, 2019, **43**, 567–584.

32 S. T. Wu, Y. P. Wang and C. X. Xu, *Chin. J. Anal. Chem.*, 2017, **45**, 965–972.
33 S. S. Sun and W. F. McDonough, *Geol. Soc. Lond. Spec. Publ.*, 1989, **42**, 313–345.
34 T. E. Krogh, *Geochim. Cosmochim. Acta*, 1973, **37**, 485–494.
35 H. Gerstenberger and G. Haase, *Chem. Geol.*, 1997, **136**, 309–312.
36 J. S. Stacey and J. D. Kramers, *Earth Planet. Sci. Lett.*, 1975, **26**, 207–221.
37 A. H. Jaffey, K. F. Flynn, L. E. Glendenin, W. C. Bentley and A. M. Essling, *Phys. Rev.*, 1971, **4**, 1889–1906.
38 R. H. Steiger and E. Jäger, *Earth Planet. Sci. Lett.*, 1977, **36**, 359–362.
39 S. T. Wu, Y. H. Yang, H. Wang, C. Huang, L. W. Xie and J. H. Yang, *At. Spectrosc.*, 2020, **41**, 154–161.
40 S. T. Wu, M. Yang, Y. H. Yang, L. W. Xie, C. Huang, H. Wang and J. H. Yang, *Int. J. Mass Spectrom.*, 2020, **456**, 116394.
41 Z. Y. Li, Q. X. Xia and Y. X. Liu, *Lithos*, 2023, **440/441**, 107028.
42 K. R. Ludwig, *ISOPLOT 3.0: A Geochronological Toolkit for Microsoft Excel*, Berkeley Geochronology Center, Special Publication, 2003, vol. 4, p. 71.
43 L. J. Millonig, R. Albert, A. Gerdes, D. Avigad and C. Dietsch, *Earth Planet. Sci. Lett.*, 2020, **552**, 116589.
44 M. Burisch, A. Gerdes, L. D. Meinert, R. Albert, T. Seifert and J. Gutzmer, *Earth Planet. Sci. Lett.*, 2019, **519**, 165–170.